Amplitude-based DAS logging: turning DAS VSP amplitudes into subsurface elastic properties

Vladimir Kazei[1], Konstantin Osypov[1], Ezzedeen Alfataierge[2], Andrey Bakulin[2]*
1 – Aramco Services Company, Houston, 2 - EXPEC Advanced Research Center, Saudi Aramco

SUMMARY

Distributed acoustic sensing (DAS) is gaining popularity for conducting vertical seismic profiling (VSP). Being a spatially densely sampled recording of the acoustic wavefield, DAS data provides a truly continuous measurement along the well instead of a discrete array of points with geophone VSP. This feature of DAS is remaining underutilized by conventional processing flows. We develop a simple theory that relates DAS and conventional geophone measurements to potential and kinetic energies, correspondingly. Balancing the DAS-recorded energy along the well leads us to a simple algorithm for inversion of zero-offset DAS VSP. The resolution of the final algorithm is defined by DAS channel spacing and gauge length rather than by the frequencies of the seismic wavelet. We validate the algorithm in a synthetic example, inspired by a complex near-surface model from the desert environment, and a field data test from the instrumented test well.

INTRODUCTION

DAS recently emerged as a viable alternative to recording by geophones in VSP application (Mateeva et al., 2013). The fundamental difference between DAS and geophone measurements lies in the fact that strain (or strain rate) is measured instead of particle velocity (or acceleration). The DAS technology enabled previously prohibitively expensive dense channel spacing in seismic surveys. This dense spacing in the DAS channels potentially enables resolving the local properties of the elastic subsurface along the fiber at the resolution primarily limited by gauge length and channel spacing. Current practical applications are computationally expensive being based on full-waveform inversion (Podgornova et al., 2017; Egorov et al., 2018; Eaid et al., 2020). To decouple elastic parameters from seismic reflections rich illumination angle content and frequency content is necessary (Kazei and Alkhalifah, 2018; Podgornova et al., 2018) and/or multicomponent measurements are desirable (Kazei and Alkhalifah, 2019).

DAS provides a unique opportunity for direct inversion of the wavefields recorded in situ for the rock properties near the DAS fiber. Mateeva and Zwartjes (2017) noted the correlation between DAS measurements and the vertical velocity and density profiles from sonic logs and proposed a theoretical explanation based on pressure preservation along the well. Pevzner et al. (2020) suggested an alternative theory based on energy flux preservation along the well and demonstrated similar correlations between logs and DAS RMS amplitudes of first arrivals of teleseismic events.

In both publications constant density one-way wave equation was inherently used as additional assumption in the derivation, which can accommodate only a single wave arrival in inversion. Kazei & Osypov (2021), inspired by the work of Pevzner et al. (2020), developed a computationally efficient approach utilizing full DAS-recorded wavefields for prompt estimation of density and velocity in zero-offset VSP geometry. Here we extend their approach and apply it to field data from Aramco test well in Houston.

THEORY

Our theory can be summarized in the following points:

1. DAS measurements
In most acquisition scenarios, the data provided by DAS systems is essentially strain (e.g., Dean et al., 2017) or strain rate Martin (2018) averaged over the gauge length (GL). The GL is effectively the length of the fiber cable segment that measures the strain of the subsurface. Depending on the measurement system, the DAS measurement is usually interpreted as averaged over GL strain or strain rate. Dean et al. (2017) proposed to select gauge length as a fraction of the seismic wavelength propagating in the media. Martin (2018) outlined the effective response of the cable fragment depending on the gauge length. Merry et al. (2020) and Alfataierge et al. (2020) experimentally studied the effect of gauge length on signal-to-noise ratio arriving at a similar conclusion as Dean et al. (2017). While the SNR in the data and in the inverted elastic parameters are related, they are not the same.

Further development of DAS measurement systems leads to the appearance of submeter GL with acceptable signal-to-noise ratios. There are emerging examples of alternative DAS systems without gauge length (Fernandez-Ruiz et al., 2019). Therefore, we do not account for gauge length in our analysis.

2. The energy in DAS measurements
If we assume that the deformation is only vertical (Morse and Feshbach, 1953), then local energy in an elastic solid comprises of kinetic part E_k:

$$E_k = \frac{1}{2}\rho U_t^2 \tag{1}$$

and potential part E_p:

$$E_P = \frac{1}{2}\lambda U_z^2 = \frac{1}{2}\rho v^2 U_z^2, \tag{2}$$

where U is vertical displacement and U_t and U_z are vertical particle velocity and strain correspondingly; v and ρ are the P–wave velocity and density correspondingly.

If the motion is cyclic, then according to the virial theorem (Clausius, 1870):

$$< E_K >_t = < E_P >_t, \quad (3)$$

or

$$< U_t^2 >_t = v^2 < U_z^2 >_t , \quad (4)$$

where $<.>_t$ denotes averaging over a single period. Seismic recording can be considered cyclic.

Equation 4 enables inverting seismic recording amplitudes for velocity directly from measurements of DAS (U_z) and geophone (U_t) data.

3. Energy flux

Energy does not disappear or accumulate inside an elastic medium during wave propagation. Hence, energy flux is constant with respect to vertical location (e.g., Claerbout, 1976; Waterman, 1978). Original energy flux (Morse and Feshbach, 1953):

$$S = -\lambda U_z U_t \quad (5)$$

accommodates arbitrary direction of wave propagation. If we assume the absence of residual and preceding wavefields, then all the energy emitted by the source has propagated through the medium and

$$\int_0^{+\infty} S dt = const. \quad (6)$$

Again, if geophone and DAS data are available, $\lambda = \rho v^2$ can be directly reconstructed from the equation (6). In principle, combining equations (4) and (5) enables estimation of both velocity and density, provided data from geophone and DAS are available. In practice, geophones cannot be placed as dense as DAS recording channels. Therefore, we focus on property inversion with DAS only.

Pevzner et al. (2020) expressed the energy flux traveling along the well for an earthquake first arrivals as (so-called *P*-flux):

$$W = \rho v^3 U_z^2 \quad (7)$$

and used conservation principle

$$\int_0^T W dt = const , \quad (8)$$

to reconstruct ρv^3 along the well. We call this quantity ρv^3 "DAS impedance" as it controls *in situ* amplitudes of the DAS measurements. Note that this impedance is different in nature from conventional acoustic impedance ρv, which could be related to geophone amplitudes in the same context.

Pevzner et al. (2020) used a one-way wave equation

$$U_t = v U_z, \quad (9)$$

focusing on energy analysis of first arrivals that are reasonably well described by such approximation. In contrast, equation (8) is more general and can also accommodate later arrivals. Besides, *P*-flux (7) is not preserved at reflector positions.

To extend the concept of P-flux to full recorded DAS waveforms let us assume that we were able to separate full wavefield into up and down going parts. For each of these wavefields, equation (7) essentially describes the transfer of potential energy. In the downgoing part of the wavefield, the energy (2) is going down with the velocity v. Therefore, the equation (7) expresses the downgoing flux of potential energy. P-flux is not preserved, as the full energy balance is:

$$\left(< E_p^{\downarrow} + E_k^{\downarrow} - E_p^{\uparrow} - E_k^{\uparrow} >_t\right) v(z) = const(z), \quad (10)$$

where arrows denote the direction of energy density propagation. Using the equation (3), equation (10) can be rewritten:

$$\left(< E_p^{\downarrow} - E_p^{\uparrow} >_t\right) v(z) = const(z). \quad (11)$$

Equation (11) allows establishing a method for the inversion of distributed data for DAS impedance based on potential energy flux. Therefore, we generalize Pevzner et al. (2020) approach to accommodate both up- and downgoing waves. In practice, we suggest using up and down separation of wavefields.

METHOD

Our method consists of four main steps summarized below.

1. Geometrical spreading correction

We consider an application to zero-offset (ZO) VSP acquired with vertical DAS cable. To further simplify, we reduce the 2D synthetic and 3D real data to their 1D approximation. Since we work with energies, the correction can be limited to the amplitude correction of the data. This correction can be performed with tailored gain control in practice. We limit ourselves to a simple multiplication of strain seismograms with the square root of time for this proof-of-concept study. This correction also helps to match the amplitudes of multiples to 1D approximation.

2. Up-down wavefield separation

Similar to geometric spreading correction, we employ the simplest up-down separation in the f-k domain. The first and third quadrants of the f-k spectrum are considered upgoing, and the second and third quadrants are considered downgoing energy. For VSP data, this type of separation is straightforward, but several more sophisticated approaches exist.

3. Estimating energy of upgoing and downgoing fields

The computation of the RMS amplitude of the wavefield is a straightforward procedure, unlike the recording interval's choice. Pevzner et al. (2020) considered the first arrivals for his procedure. In our approach, we consider the entire length of seismograms.

4. Impedance transformation

After RMS amplitudes are computed, we transform them into the relative DAS impedance:

$$\rho v^3 \propto \left(\left\| U_{DAS}^{\downarrow} \right\|_2^2 - \left\| U_{DAS}^{\uparrow} \right\|_2^2 \right)^{-1}, \quad (12)$$

where UDAS and UDAS are down- and up-going DAS-measured strains. Equation (12) requires a single calibration point to arrive at the absolute DAS impedance values, where the impedance must be known from other sources.

SYNTHETIC EXAMPLE

Let us evaluate the inversion using synthetic modeling of smart DAS uphole (Bakulin et al., 2017). The elastic model (Figure 1) is inspired by actual complex near-surface in a desert environment (Alexandrov et al., 2015). The ZO VSP data were generated in Dhahran and then inverted blindly in Houston. Forward modeling was based on a pseudo-spectral 2D elastic modeling with a grid spacing of 1 m. Computed point strains were averaged during the final stage of the modeling to replicate DAS measurement with 5 m gauge length. Ricker wavelet with 50 Hz central frequency was used and one second of data were inverted. The synthetic model captures the main complexity of the near surface in the desert environment, including low velocities near the surface and alternating high- and low-velocity layers with strong contrasts. The influence of this complex velocity is evident in the data as we see a significant reduction in amplitude after wave propagation through the shallow high-velocity layer.

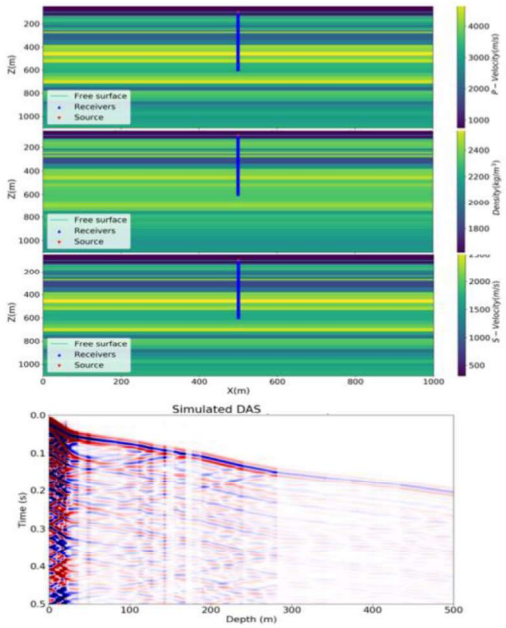

Figure 1: Elastic near-surface model and simulated for 5 m gauge length DAS wavefield (averaged strain)

Inverted DAS impedance using the proposed energy-driven provides a more accurate profile for this example (Figure 2) compared to Pevzner et al. (2020). Their method strongly overpredicts impedance in the deeper part while underpredicting in the shallow part. In contrast, our approach only deviates in the first 150 m interval. Perhaps, near-field effects and reverberating near-surface events may play a role. If we ignore relatively small changes in density, we can interpret cubic root from DAS impedance as a direct estimate of velocity. Large velocity contrasts lead to significant inaccuracies when doing geometrical spreading corrections. Nevertheless, most jumps in the impedance are reasonably well recovered. Estimates in the near field (first ~30-70 m) Wave separation leads to some smoothing of the boundaries due to known boundary artifacts. However, due to dense sampling of DAS channels spatial aliasing is not an issue here. Better separation methods can further improve the DAS impedance accuracy.

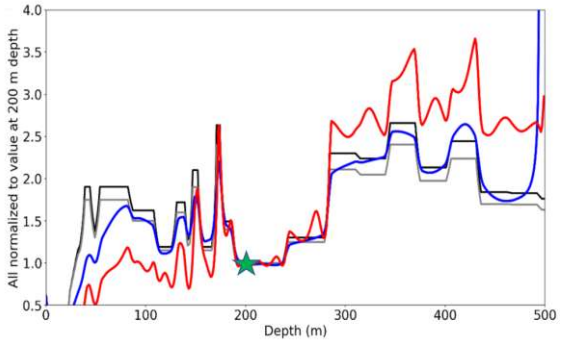

Figure 2: P-wave velocity v (grey), the cubic root from DAS impedance $(v^3\rho)^{1/3}$ used for simulation (black) and reconstructed from the synthetic data using P-flux (red), and energy-driven DAS amplitude inversion (blue). Calibration point is marked by green star.

FIELD DATA EXAMPLE

Let us apply the new method to field data recorded in instrumented well at Aramco Houston Research center. Layered subsurface is expected in the area. Test well is instrumented with DAS cable cemented behind casing from the surface down to 500 m. We select a subset of the data 150-400 m with the highest data quality for inversion. Dataset with 4 m gauge length suggested by Alfataierge et al. (2020) as most perspective. Wireline logs of density and P-wave velocity were used to build a synthetic model (Figure 3a, b) and simulate wave propagation with 50 Hz Ricker wavelet. Comparison of synthetic data and actual field data is shown in Figures 3c and 3d, respectively.

Inversion results for synthetic records retrieve most amplitude variations in the smoothed log profile of the DAS impedance, while field data collected with the GL equal to 4 m gets the general profile of the subsurface (Figure 4). The near-surface part of the profile is not well retrieved most likely due to lateral heterogeneity.

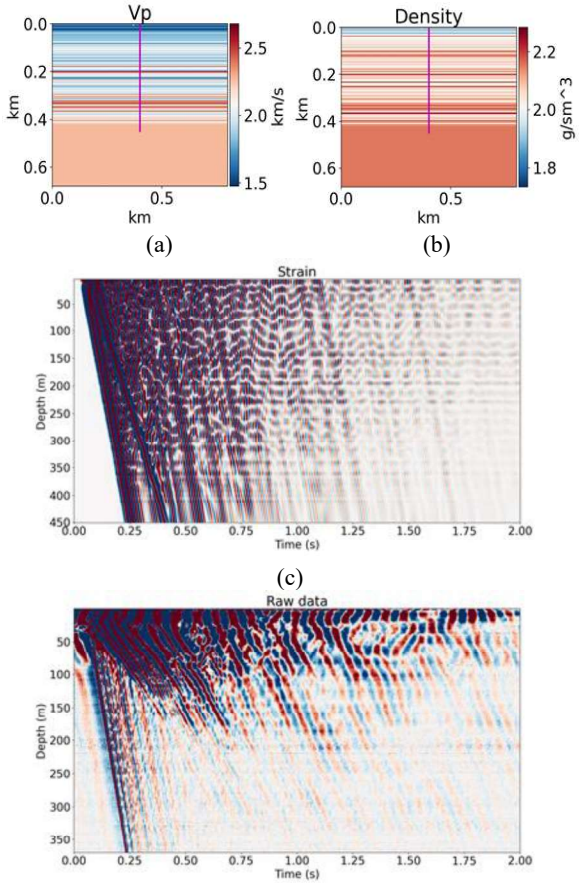

Figure 3: 1D velocity model built from well logs: (a) *P*-wave velocity, (b) density. *S*-wave velocity is derived by assuming constant Poisson ratio of 0.25. DAS wavefield: (c) simulated point strain from synthetics, (d) raw DAS field data recorded using GL = 4 m.

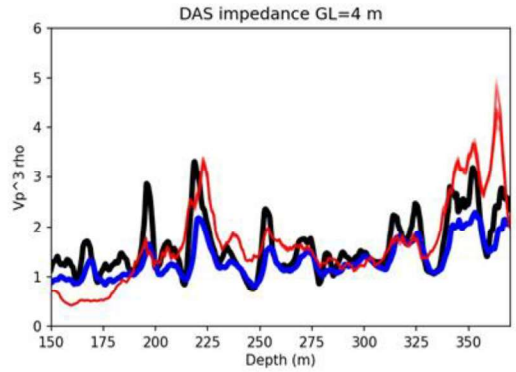

Figure 4: Inverted DAS impedance (values normalized) from synthetic data (blue), from field data (red). Black curve shows ground truth obtained from upscaled wireline logs (4 m averaging).

DISCUSSION

DAS resolution

DAS resolution is defined by spatial sampling and gauge length. The signal bandwidth does affect the resolution directly. It is important for the inversion assumptions validity. In particular, geometrical spreading comes from the ray theory and the ray theory works better for higher frequencies. Geometrical spreading correction might not be necessary if the source is remote and the incident waves can be approximated by plane waves. The other important aspect is that the surface and trapped waves present a larger relative portion of the wavefield at lower frequencies. These types of waves can serve as secondary sources and deteriorate the resolution of the model parameters.

Fidelity of the amplitude and coupling

It is assumed that DAS fiber is perfectly coupled to the formation, so correct in-situ formation strain is captured by fiber-optic cable. Such assumption may hold for smart DAS uphole where fiber is cemented in place by design (Bakulin et al., 2017). It is also applicable to cemented fiber behind casing, as in the field example. It should not be taken for granted and revisited for other types of fiber deployments that may be more frequently used in production and injection wells (fiber on tubing or in wireline, etc.).

CONCLUSIONS

We developed a simple theory and a concept for amplitude-based DAS logging that uses the entire wavefield recorded during VSP surveys instead of the first arrivals as in previous attempts. DAS logging transforms DAS VSP measurement into a subsurface profile of density and velocity or their combination. These profiles resemble filtered acoustic logs, hence explaining the title. The new method comprises of up-down wave decomposition, and geometrical spreading correction applied directly to DAS data. This amplitude pre-processing enables quantitative inversion of energies directly into relative DAS impedance along the borehole. A single calibration point is required to obtain absolute impedance. We validated the concept using synthetic and field datasets. A reasonable estimate of DAS impedance can be retrieved in both models. Synthetic dataset represented a smart DAS uphole survey from the desert environment. Despite challenging high-contrasting sections, the method does an excellent job mapping the velocity layer boundaries and capturing the thin layer velocity inversions, although underpredicted in the shallowest sections.

ACKNOWLEDGMENTS

We thank Mustafa Ali, Weichang Li, Harold Merry and Max Deffenbaugh for inspiring technical input.

REFERENCES

Alexandrov, D., Bakulin, A., Burnstad, R., and B. Kashtan, 2015, Improving imaging and repeatability on land using virtual source redatuming with shallow buried receivers: Geophysics, **80**, no. 2, Q15–Q26, doi: https://doi.org/10.1190/geo2014-0373.1.

Alfataierge, E., A. Aldawood, A. Bakulin, R. R. Stewart, and H. Merry, 2020, Influence of gauge length on das VSP data at the Houston Research Center test well: SEG Technical Program, Expanded Abstracts, 505–509, doi: https://doi.org/10.1190/segam2020-3419066.1.

Bakulin, A., Golikov, P., Smith, R., Erickson, E., Silvestrov, I., and M. Al-Ali, 2017, Smart DAS upholes for simultaneous land near-surface characterization and subsurface imaging: The Leading Edge, **36**, 1001–1008, doi: https://doi.org/10.1190/tle36121001.1.

Claerbout, J., 1976, Fundamentals of geophysical data processing: Citeseer.

Clausius, R., 1870, Xvi. on a mechanical theorem applicable to heat: The London, Edinburgh, and Dublin Philosophical Magazine and Journal of Science, **40**, 122–127, doi: https://doi.org/10.1080/14786447008640370.

Dean, T., T. Cuny, and A. H. Hartog, 2017, The effect of gauge length on axially incident p-waves measured using fibre optic distributed vibration sensing: Geophysical Prospecting, **65**, 184–193, doi: https://doi.org/10.1111/1365-2478.12419.

Eaid, M. V., S. D. Keating, and K. A. Innanen, 2020, Multiparameter seismic elastic full-waveform inversion with combined geophone and shaped fiber-optic cable data: Geophysics, **85**, no. 6, R537–R552, doi: https://doi.org/10.1190/geo2020-0170.1.

Egorov, A., J. Correa, A. Bona, R. Pevzner, K. Tertyshnikov, S. Glubokovskikh, V. Puzyrev, and B. Gurevich, 2018, Elastic full-waveform inversion of vertical seismic profile data acquired with distributed acoustic sensors: Geophysics, **83**, no. 3, R273–R281, doi: https://doi.org/10.1190/geo2017-0718.1.

Fernandez-Ruiz, M. R. M. L. Costa, and H. F. Martins, 2019, Distributed acoustic sensing using chirped-pulse phasesensitive otdr technology: Sensors, **19**, 4368, doi: https://doi.org/10.3390/s19204368.

Kazei, V., and T. Alkhalifah, 2018, Waveform inversion for orthorhombic anisotropy with P-waves: Feasibility & resolution: Geophysical Journal International, **213**, 963–982, doi: https://doi.org/10.1093/gjihttps://doi.org//ggy034.

Kazei, V., and T. Alkhalifah, 2019, Scattering radiation pattern atlas: What anisotropic elastic properties can body waves resolve?: Journal of Geophysical Research, Solid Earth, **124**, 2781–2811, doi: https://doi.org/10.1029/2018JB016687.

Kazei, V. and K. Osypov, 2021, Inverting DAS data using energy conservation principles: Interpretation (submitted).

Kohn, D., D. De Nil, A. Kurzmann, A. Przebindowska, and T. Bohlen, 2012, On the influence of model parametrization in elastic full waveform tomography: Geophysical Journal International, **191**, 325–345, doi: https://doi.org/10.1111/j.1365-246X.2012.05633.x.

Martin, E. R., 2018, Passive imaging and characterization of the subsurface with distributed acoustic sensing: PhD thesis, Stanford University.

Mateeva, A., J. Lopez, J. Mestayer, P. Wills, B. Cox, D. Kiyashchenko, Z. Yang, W. Berlang, R. Detomo, and S. Grandi, 2013, Distributed acoustic sensing for reservoir monitoring with vsp: The Leading Edge, **32**, 1278–1283, doi: https://doi.org/10.1190/tle32101278.1.

Mateeva, A., and P. Zwartjes, 2017, Depth calibration of das VSP channels: a new data-driven method: 79th EAGE Conference and Exhibition 2017, 1–5, doi: https://doi.org/10.3997/2214-4609.201701201.

Merry, H., W. Li, M. Deffenbaugh, and A. Bakulin, 2020, Optimizing distributed acoustic sensing (das) acquisition: Test well design and automated data analysis: SEG Technical Program, Expanded Abstracts, 520–524, doi: https://doi.org/10.1190/segam2020-3419338.1.

Pevzner, R., B. Gurevich, A. Pirogova, K. Tertyshnikov, and S. Glubokovskikh, 2020, Repeat well logging using earthquake wave amplitudes measured by distributed acoustic sensors: The Leading Edge, **39**, 513–517, doi: https://doi.org/10.1190/tle39070513.1.

Podgornova, O., S. Leaney, and L. Liang, 2018, Resolution of VTI anisotropy with elastic full-waveform inversion: Theory and basic numerical examples: Geophysical Journal International, **214**, 200–218, doi: https://doi.org/10.1093/gjihttps://doi.org//ggy116.

Podgornova, O., S. Leaney, S. Zeroug, and L. Liang, 2017, On full-waveform modeling and inversion of fiber-optic VSP data: SEG Technical Program, Expanded Abstracts, 6039–6043, doi: https://doi.org/10.1190/segam2017-17652912.1.

Waterman, P., 1978, Matrix theory of elastic wave scattering. II. A new conservation law: The Journal of the Acoustical Society of America, **63**, 1320–1325, doi: https://doi.org/10.1121/1.381884.